The mean physical and optical properties of regional haze dominated by biomass burning aerosol measured from the C-130 aircraft during SAFARI 2000

Jim M. Haywood,[1] Simon R. Osborne,[1] Pete N. Francis,[1] Andreas Keil,[1]
Paola Formenti,[2,3] Meinrat O. Andreae,[2] and Paul H. Kaye[4]

[1]   Instrumentation on the Met Office C-130 aircraft measured aerosol physical and optical properties during the Southern African Regional Science Initiative (SAFARI 2000) in September 2002 while flying from Windhoek, Namibia. Filter measurements of aged regional haze suggest a ratio of apparent elemental carbon (EC_a) to organic carbon (OC) of 0.12 ± 0.02 and mass fractions of 5% EC_a, 25% inorganic compounds, and 70% organic matter (OC plus associated elements). The submicron size distribution of aged regional haze may be fitted with three lognormal distributions with geometric mean radii (r_n) of 0.12 ± 0.01, 0.26 ± 0.01, and 0.80 ± 0.01 μm and geometric standard deviations (σ) of 1.3 ± 0.1, 1.5 ± 0.1, and 1.9 ± 0.4. Measurements over 2500 km from the emission region show similar r_n and σ for the smallest two modes, while the third mode is absent presumably as a result of sedimentation. At a wavelength (λ) of 0.55 μm, effective medium approximations suggest a refractive index of $1.54 - 0.018i$ for aged regional haze aerosol. The single scattering albedo ($\omega_{o\lambda}$) derived using this refractive index and measured size distributions are consistent with those from the nephelometer and Particle Soot Absorption Photometer (PSAP). The optical parameters for aged regional haze a few days old are specific extinction coefficient ($k_{e\lambda=0.55}$) of 5.0 ± 0.8 m^2 g^{-1}, asymmetry factor ($g_{\lambda=0.55}$) of 0.59 ± 0.02, and $\omega_{o\lambda=0.55}$ of 0.91 ± 0.04. Measurements of fresh biomass burning aerosol a few minutes old show smaller more absorbing particles. Vertical profiles of carbon monoxide, aerosol concentration, and aerosol scattering show a good correlation. Over land, aerosols become well mixed in the vertical from the surface to approximately 500 hPa. Over ocean, the aerosols can be separated from underlying stratocumulus cloud by a clear gap and a strong inversion, which may limit the indirect effect.   *INDEX TERMS:* 0305 Atmospheric Composition and Structure: Aerosols and particles (0345, 4801); 0360 Atmospheric Composition and Structure: Transmission and scattering of radiation; 0365 Atmospheric Composition and Structure: Troposphere—composition and chemistry; 3359 Meteorology and Atmospheric Dynamics: Radiative processes; 9305 Information Related to Geographic Region: Africa; *KEYWORDS:* atmospheric aerosol, biomass burning, SAFARI 2000, aerosol optical properties

Citation: Haywood, J. M., S. R. Osborne, P. N. Francis, A. Keil, P. Formenti, M. O. Andreae, and P. H. Kaye, The mean physical and optical properties of regional haze dominated by biomass burning aerosol measured from the C-130 aircraft during SAFARI 2000, *J. Geophys. Res.*, *108*(D13), 8473, doi:10.1029/2002JD002226, 2003.

1.   Introduction

[2]   The *IPCC* [2001] and *Ramaswamy et al.* [2001] suggest that biomass burning contributes a significant but poorly quantified direct radiative forcing of climate, quoting a best guess estimate of -0.2 W m^{-2}, with a factor of 3

uncertainty, and a "very low" level of scientific understanding. Much of the uncertainty in the radiative forcing comes from uncertainties in the aerosol optical parameters and the spatial distribution of the aerosol in both the horizontal and vertical [e.g., *Penner et al.*, 2001; *Haywood and Boucher*, 2000; *Haywood and Ramaswamy*, 1998; *Hobbs et al.*, 1997].

[3]   The Met Office C-130 aircraft was based in Windhoek, Namibia during the Southern African Regional Science Initiative (SAFARI) 2000 measurement campaign with a primary objective of measuring the radiative properties and direct radiative effect of aerosols produced from biomass sources. This study concentrates on measurements and modeling of the physical and optical properties of aged regional haze rich in biomass burning aerosol, issues that

---

[1]The Met Office, Bracknell, UK.
[2]Biochemistry Department, Max Planck Institute for Chemistry, Mainz, Germany.
[3]Now at Centre of Geophysics, University of Evora, Evora, Portugal.
[4]Science and Technology Research Centre, University of Hertfordshire, Hatfield, UK.

are of central importance in refining estimates of the direct radiative forcing. A further study by *Haywood et al.* [2003a] investigates the consistency of airborne and surface-based remote sensing measurements. In this study, sections 2 and 3 describe the instrumentation for measuring aerosol particles and flight patterns performed during the campaign. Sections 4 and 5 describe the measured chemical composition and refractive indices derived from the chemistry measurements. Section 6 presents the measured aerosol size distributions and section 7 shows how these measurements are used to determine the optical parameters, and compares the optical parameters with those measured directly. Section 8 describes measurements of the vertical profiles of the aerosol concentration and scattering. Section 9 provides a discussion and conclusions.

2. Relevant Instrumentation

[4] The C-130 was equipped with the standard instrumentation detailed by *Johnson et al.* [2001]. In addition, the following equipment was fitted specifically for measuring the size distributions, chemical composition, and optical and physical properties of aerosols. Aerosol size distributions between 0.05 and 1.5 μm radius were determined with a Particle Measuring System (PMS) Passive Cavity Aerosol Spectrometer Probe 100X (PCASP). A Fast Forward Scattering Spectrometer Probe (FFSSP) developed from a PMS FSSP was used to measure aerosol and cloud particles between 1 and 23.5 μm radius. The Small Ice Detector (SID) [*Hirst et al.*, 2001], was also fitted. SID was originally designed to measure particle shape, size, and concentration for discrimination between supercooled water drops and ice crystals in the radius range 0.5–12 μm, however, aerosol particles are also detectable. Aerosol chemistry was determined from isokinetic sampling onto filter substrates. Two filter packs were used: quartz filter packs for apparent elemental carbon (EC_a) (see section 4 below for a definition of this parameter) and organic carbon (OC) analysis via a thermal-optical transmission (TOT) technique, and Teflon packs for major cation and anion chromatography. These packs had Nuclepore filters mounted in front of them to fractionate the particles into a coarse (onto the Nuclepore) and fine (onto the Teflon or quartz) fraction, the approximate cut between coarse and fine particles being 0.65 μm aerodynamic radius. The sampling system has been described in detail by *Andreae et al.* [2000]. The quartz filters were subsequently analyzed for EC_a and OC, while the Teflon and Nuclepore filters were analyzed for water-soluble ions and inorganic elemental components [*Formenti et al.*, 2003]. Particulate absorption of radiation of wavelength 0.567 μm was measured with a Radiance Research Particle Soot Absorption Photometer (PSAP). Aerosol scattering was determined at three wavelengths (0.45, 0.55, and 0.70 μm) with a TSI 3563 nephelometer. Carbon monoxide measurements (resonance-fluorescence technique, developed by FZ Jülich) were made throughout the SAFARI campaign.

3. Aircraft Flight Patterns

[5] The aircraft performed 8 dedicated flights from Windhoek, Namibia during the period 5–16 September
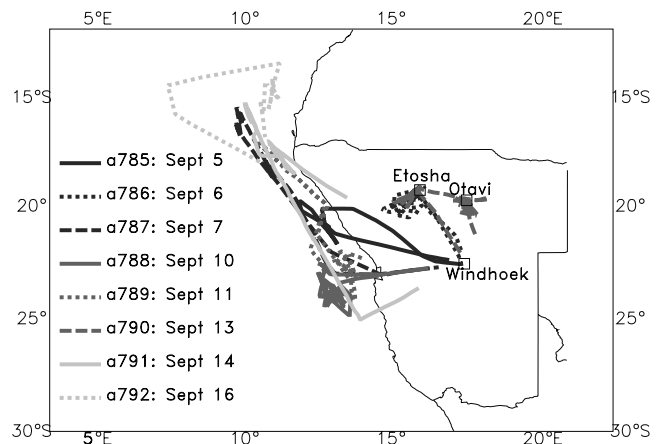

Figure 1. Map showing the geographical location of the flights performed by the C-130 during SAFARI 2000. The approximate positions of Windhoek, Etosha, and Otavi are marked. The geopolitical outline of Namibia is also shown.

2000, with two additional scientific transit flights Windhoek-Ascension Island on 2 and 18 September 2000 for a total of approximately 80.5 flight hours. Figure 1 shows that the majority of the flights were performed over the ocean off the coast of Namibia and Angola where the surface characteristics are relatively well known which is beneficial for radiative closure studies [e.g., *Hignett et al.*, 1999; *Haywood et al.*, 2001a, 2001b]. Generally, the aircraft was operating in the region of outflow from the Southern African anticyclone and was downwind of most of the significant sources of aerosol. Thus the aerosol was typical of aged regional haze that is advected westward off the coast of Southern Africa toward South America. Figure 2 shows Total Ozone Mapping Spectrometer (TOMS) images of the UV-absorbing Aerosol Index during the campaign. Although there is significant variability, Figures 1 and 2 show that the C-130 was generally operating close to the maximum in the aerosol index.

[6] The dedicated flight patterns typically consisted of straight and level runs (SLRs) within, below, and above the aerosol layer, with profiles in between. The SLRs within the aerosol layer concentrated on in situ sampling of the aerosol size distributions with the PMS probes and SID, collection of filter samples to determine aerosol chemistry, and in situ measurements of the scattering and absorption coefficients with the nephelometer and PSAP. The profiles from below the aerosol layer to above the aerosol layer determined the vertical profile of the aerosol concentrations.

[7] In addition to sampling aged aerosol, fresh biomass aerosol was sampled on 13 September in a plume over a large human-induced biomass fire in agricultural land near Otavi in northern Namibia. This fire had spread from the agricultural land in the valley to the cerrado and scrubland on the surrounding hills and therefore consisted of a mixture of fuel sources. The burn scar was approximately 5 km^2, and consisted of both flaming and smoldering combustion sources. In this case the flight pattern consisted of measurements directly over the plume, at altitudes down to 208 m
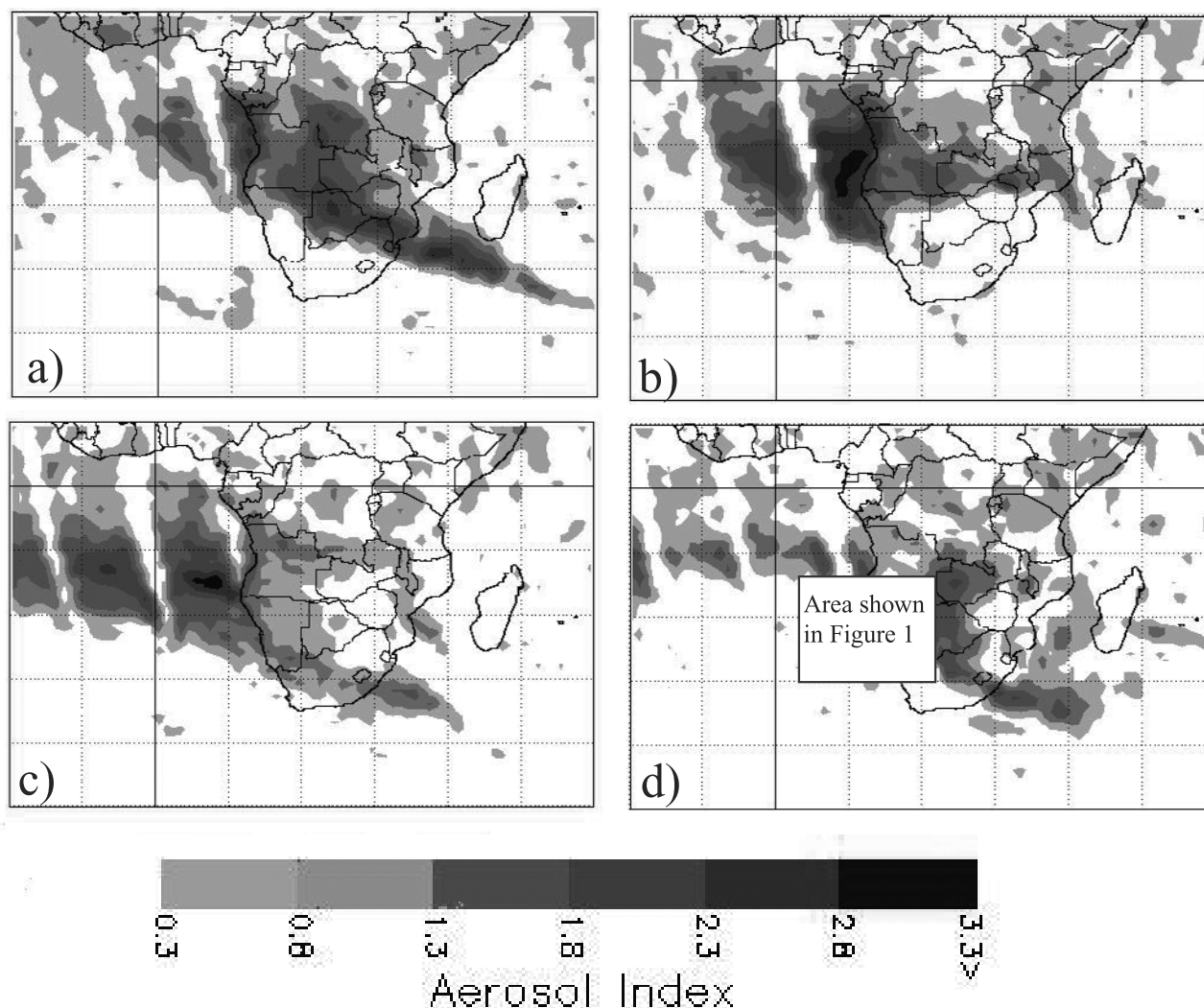
Figure 2. TOMS image of the aerosol index [*Herman et al.*, 1997] on (a) 5 September 2000, (b) 9 September 2000, (c) 13 September 2000, and (d) 16 September 2000. The approximate area corresponding to the operating region shown in Figure 1 is shown by the black box in panel (d). The vertical stripes in the aerosol index show missing data owing to the finite viewing swath-width of the instrument. Original images courtesy of NASA GSFC.

AGL and measurements across the plume for a distance of approximately 70 km downwind.

4. Aerosol Chemical Composition

[8] Fine particle (<0.65 μm radius) EC_a and OC were determined from the quartz filters using a TOT technique (Formenti et al., submitted manuscript, 2002). This technique consists in inducing, by a stepped temperature gradient, the thermal evolution of the carbonaceous species present on the filter substrate. Simultaneously, the changes in transmissivity through the filter are measured, and related to the progressive evolution of OC (at lower temperatures) and then elemental carbon [*Birch and Cary*, 1996]. A complete discussion of the interpretation of the measurements and the implied caveats is given by *Formenti et al.* [2003]. Here we note that the thermal-optical technique does not measure blackness in the optical sense, but the chemically refractory property of the carbon, which is

interpreted on the assumption that the carbon that volatilize at higher temperatures is soot-like or nearly elemental. A major uncertainty is therefore in the definition of the split between carbon to be considered as organic and that to be assigned to the elemental fraction. Intercomparison studies have shown that the accuracy on the absolute value of the elemental carbon and OC concentrations may have uncertainties up to a factor of 2 [*Chow et al.*, 2001; *Schmid et al.*, 2001]. However, a previous intercomparison between the atmospheric concentrations in an urban environment of the elemental carbon obtained by the TOT instrument used in this study and that from a light reflection instrument has shown agreement within few percent (W. Maenhaut, personal communication, 2001). Errors are expected to be larger for aerosol containing a large biomass burning fraction, where a significant amount of the organic component is high-molecular-weight material with refractory properties similar to elemental carbon [*Mayol-Bracero et al.*, 2002], so that some refractory OC may be included in
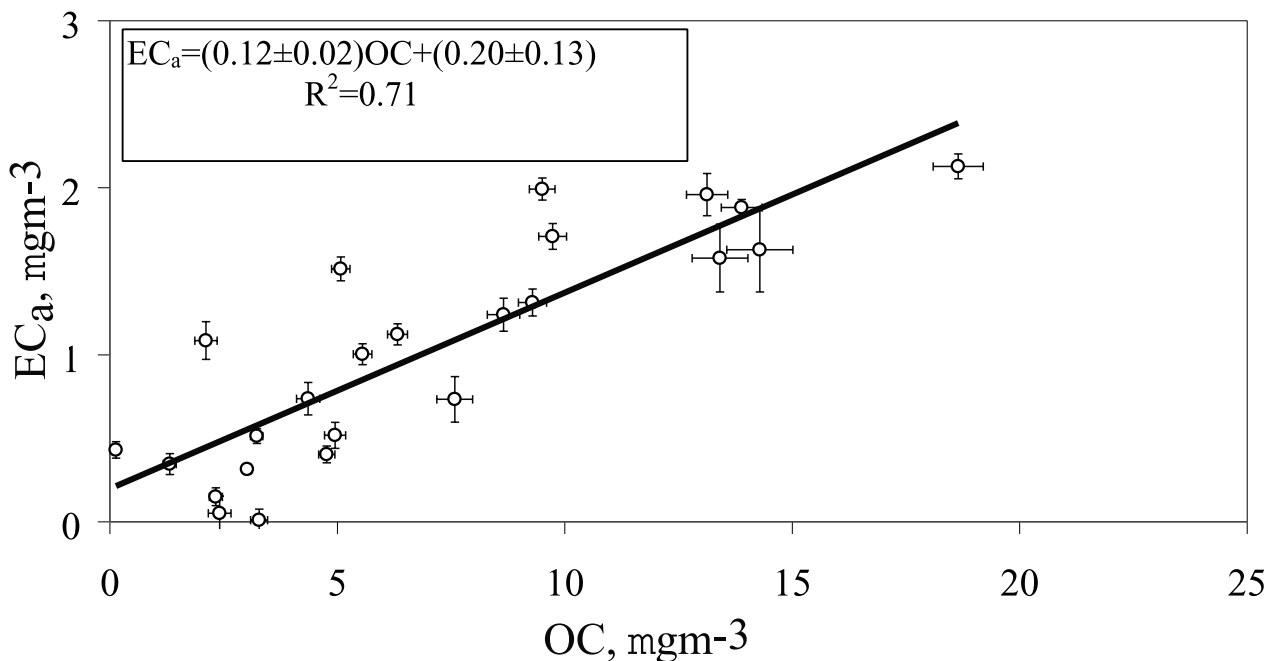
$$EC_a = (0.12 \pm 0.02)OC + (0.20 \pm 0.13)$$
$$R^2 = 0.71$$

Figure 3. A regression analysis of EC_a against OC speciation from filters collected during each of the flights in SAFARI 2000. For aged aerosol, the mass ratio $M_{ECa/OC} = 0.12$.

the EC_a. Furthermore, light absorption in biomass-rich aerosol is due to both, soot-like "elemental" carbon and colored organic matter ("brown carbon"). For the time being, we retain EC_a as an operationally defined parameter representing the optically absorbing, refractory carbonaceous aerosol, and caution that its chemical identity is not well defined. A description of the artifacts leading to overestimation or underestimation of BC for biomass aerosols is given by *Reid et al.* [1998a]. A full description of the TOT instrument, technique, and method used to minimize the artifacts are given in Formenti et al. (submitted manuscript, 2002), and *Schmid et al.* [2001].

[9] The regression analysis shown in Figure 3 reveals that EC_a and OC are correlated ($r^2 = 0.71$), with a mean EC_a/OC mass fraction, $M_{ECa/OC}$, for aged aerosol of 0.12. The effects of aging upon the refractive indices, size distributions, and single scattering albedo are further investigated in sections 5, 6, and 7, respectively.

[10] In addition to EC_a and OC, the aged regional haze contains inorganic compounds as well as hydrogen, oxygen and nitrogen associated with the OC. The filter measurements may be combined with aerosol mass <0.65 μm derived from the PCASP [*Formenti et al.*, 2003]. The difference in the fine particle mass (estimated from the filter measurements as sum of soil dust, sea salt, ammonium sulfate, EC_a, and organic matter) and the mass calculated by the PCASP by integration over radii <0.65 μm for identical sampling periods enables estimation of the mass of the additional organic matter (mainly H, O, and N) associated with the OC. These measurements suggest that the mass ratio of total organic matter to the mass of OC alone, $M_{OM/OC}$ is approximately 1.5, and that inorganic components make up approximately 25% of the total aerosol mass. Assuming that EC_a represents the absorbing component in the fine particle mass, the ratio of the absorbing mass to the

scattering mass may be calculated. These calculations and assumptions yield a $M_{ECa/total}$ of approximately 0.05. This ratio is used in calculations of the refractive index for aged regional haze in the next section.

5. Aerosol Refractive Index

[11] Determining the composite refractive index for the aerosols is not straightforward, as there are many different mixing rules for determining effective media [e.g., *Chýlek et al.*, 1988], and many different densities may be assumed for EC [e.g., *Horvath*, 1993]. Furthermore, we cannot be sure what fraction of the EC_a in our aerosols is actually soot-like material (subgraphitic material originating in flames) and what fraction is contributed by refractory, light-absorbing organic matter. The latter has properties entirely different from the carbon soot whose physical properties are usually taken as representative of EC [*Mayol-Bracero et al.*, 2002]. For the sake of consistency with previous studies, we assume EC_a to have the same properties as EC. The validity of this assumption is then examined by comparing the optical parameters, in particular $\omega_{o\lambda}$, obtained by this technique with those derived from in situ measurements (section 7).

[12] For our measurements and calculations to be of maximum use to the modeling community, two simple mixing rules are used here namely that of volume weighting the refractive indices, and the Maxwell-Garnet mixing rule. Volume weighting the refractive indices has been used in General Circulation Models (GCM) estimates of the radiative forcing due to internally mixed scattering and absorbing aerosols [e.g., *Haywood et al.*, 1997; *Myhre et al.*, 1998]. The volume weighting approach relates the effective refractive index, n_{eff}, to that of the absorbing EC component, n_{abs}, and the predominantly scattering OC component and inorganic component, n_{sca}, via the volume fraction of the

absorbing EC component, V_{abs}, and scattering component, V_{sca} via the equation:

$$n_{eff} = V_{abs}n_{abs} + V_{sca}n_{sca} \qquad (1)$$

[13] The second mixing rule that is used is the Maxwell-Garnet mixing rule, which better represents the measured absorption properties of a nonabsorbing sphere with spherical absorbing inclusions [*Chýlek et al.*, 1988]. This mixing rule has also been shown to produce results in good agreement with much more complex discrete dipole approximation calculations for closed soot clusters [*Martins et al.*, 1998]. The equation for determining n_{eff} is:

$$n_{eff}^2 = n_{sca}^2 \left(\frac{n_{abs}^2 + 2n_{sca}^2 + 2V_{abs}\left(n_{abs}^2 - n_{sca}^2\right)}{n_{abs}^2 + 2n_{sca}^2 - V_{abs}\left(n_{abs}^2 - n_{sca}^2\right)} \right) \qquad (2)$$

[14] From the measurements by *Reid and Hobbs* [1998], the density of the aerosol is assumed to be 1.35 g cm^{-3}. The density of EC has been determined to range between 0.63 g cm^{-3} for structures containing 75% empty space and 2.3 g cm^{-3} for pure graphitic structures. In these calculations, EC is assumed to have a density of 1.7 g cm^{-3}. EC is assumed to have the refractive indices used in *WCP* [1986] $n_{EC\lambda=0.55} = 1.75 - 0.44i$, and the scattering component is assumed to be nonabsorbing with a refractive index $n_{OC\lambda=0.55} = 1.53 - 0.0i$. Application of these densities and a mean $M_{EC/total}$ of 0.050 yields refractive indices for the composite aged regional haze of $1.54 - 0.018i$ for both the Maxwell-Garnet mixing rule and the volume weighting of refractive indices method. The real part of the refractive index is in agreement with that determined by *Yamasoe et al.* [1998] for biomass burning aerosol in Brazil. These calculations assume that the chemical composition does not vary between different sized particles. While these calculations involve considerable uncertainties, and cannot be used as a definitive example of "closure," this refractive index is entirely consistent with that determined from the measured size distributions and in situ measurements as discussed in section 7.

6. Aerosol Size Distributions

[15] Size distributions from the PMS probes were measured throughout the duration of the campaign. The majority of size distributions presented here represent the flight average of aerosol size distributions measured during SLRs within the aerosol plume, each of which was of at least 10 min duration.

[16] On flight a790 on 13 September the aircraft operated in fresh biomass burning aerosol from the Otavi plume. These measurements were taken directly over the fire from three SLRs at mean altitudes of between 294 and 208 m AGL, which was as low as the aircraft could safely operate because of the proximity of high ground on either side of the biomass burning plume. In this case aerosol and optical properties were considered only when the PCASP particle concentration was greater than 5000 cm^{-3} so that the measurements are representative of fresh biomass burning aerosol which is less than a few minutes old. An

upper threshold of 20,000 cm^{-3} was also applied to remove any possible effects of coincidence of the laser upon more than one particle within the PCASP [e.g., *Le Canut et al.*, 1996].

6.1. Submicron Aerosols

[17] The PCASP-100X is specifically designed for measuring aerosols in the radius range 0.05–1.5 μm. The basic principle of operation is that light from a helium-neon laser at a wavelength of 0.635 μm is incident upon single aerosol particles and the light scattered at angles between 35° and 120° is detected by a photodetector. Calibration of the PCASP-100X is performed by using latex spheres of single, well-specified sizes of known refractive index [*Knollenberg*, 1989]. The PCASP was precampaign and postcampaign calibrated and no significant drift in the sizing of the aerosol during the course of the campaign was determined. Three potential sources of error exist in the sizing of aerosols. First the refractive index of atmospheric aerosols is not identical to that of latex [e.g., *Garvey and Pinnick*, 1983]. Second, heating within the probe may cause partial evaporation of water of hydration (or volatile compounds) from the particles and therefore the measured particles may be smaller than at ambient atmospheric conditions [e.g., *Strapp et al.*, 1992]. In the work presented here, the internal heaters in the PCASP were left off to minimize evaporation of volatile OC components. Thirdly, the effects of nonsphericity may influence the scattering and lead to misclassification of the sizes [*Liu et al.*, 1992]. The mean relative humidity during the 30 SLRs used in determining the size distributions is 34% with a standard deviation of 16% and in only one out of the 30 cases does the RH exceed 57%. The University of Washington CV-580 flew out of Swakopmund, Namibia into the aged regional haze on four separate occasions and made measurements of the increase in aerosol scattering with increasing relative humidity [*Magi and Hobbs*, 2003]. At a relative humidity of 57%, the scattering increases only modestly by a mean factor of 1.07 (standard deviation 0.04), results that are similar to those of *Kotchenruther and Hobbs* [1998] who examined biomass burning aerosol in Brazil. Because of this modest response to relative humidity, the effects of relative humidity are neglected. Additional complementary measurements performed by the CV-580 during SAFARI 2000 reveal that particles in the PCASP size range are generally found to be spherical (P. Hobbs, personal communication, 2002), therefore only the effects of differing refractive indices are investigated here.

[18] The Mie scattering phase function was determined using the refractive indices of latex (1.585 − 0i) and the refractive index of aged regional haze (1.54 − 0.018i). The phase function was then integrated between angles of 35°– 120° to simulate the effective signal incident upon the photodetector. Figure 4 shows a plot of the effective PCASP response as a function of the size of the particles. The PCASP will tend to undersize the aerosol particles mainly because of attenuation of the detected signal due to particulate absorption. Table 1 shows the midpoint of the PCASP bins calculated using latex spheres and the corresponding midpoints of the bins calculated using the refractive indices of aerosol and the ratio between the midpoint radii. Figure 4
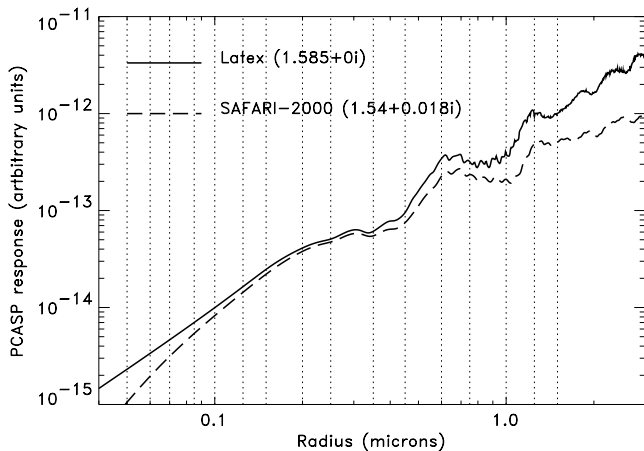
Figure 4. The PCASP response to calibration latex spheres and to aged aerosol assuming a refractive index of $1.54 - 0.018i$ at a wavelength of 0.635 μm. The lower response to the aerosol indicates that the PCASP will tend to undersize the aerosol particles.

and Table 1 show that over the particle range of approximately $0.1-0.4$ μm radius, the difference between the radii is relatively minor at approximately $5-10\%$. For radii smaller than 0.1 μm the potential error in sizing rises to $\sim 20\%$. The most significant errors occur for radii in the approximate range $0.5-1.5$ μm where the error may reach 50%. However, Mie scattering calculations using the mean size distribution (see section 6.3) reveals that particles in the $0.1-0.4$ μm radius range (PCASP bins $4-10$) contribute to over 93% of the aerosol scattering and absorption at 0.55 μm. This means that the sizing errors do not affect the derived single scattering albedo and asymmetry factor significantly. However, the specific extinction coefficient could be significantly affected because a significant proportion of the aerosol mass exists at supermicron sizes. Note that the refractive index across the size range measured by the PCASP is unlikely to remain constant as assumed in these calculations and each aerosol particle will not have exactly the same chemical composition. For example, calculations performed using refractive indices of $1.53 - 0.08i$, which is representative of dust-like particles [*WCP*, 1986], are more applicable for supermicron radii aerosols, lead to lesser errors of approximately 25% in bins 14 and 15 owing to less absorption than for the aged regional haze refractive indices. *Haywood et al.* [2003a], show that the submicron size distribution derived from the PCASP is entirely consistent with that obtained from radiometric measurements despite this correction being neglected.

[19] Because of these factors, a correction accounting for the effects of refractive index is not explicitly applied to the PCASP distributions, but rather treated as an additional source of uncertainty.

6.2. Supermicron Aerosols

[20] The results from the FFSSP in aged regional haze suggest that this probe is not able to detect and size the aerosol particles with a sufficient accuracy. Figure 5 shows the aerosol size distribution from a 30 min SLR at 2400 m

ASL during flight a789 (11 September 2000). A significant discrepancy exists between the PCASP and the FFSSP concentrations in the range $1-2$ μm radius, with the FFSSP reading typically 2 orders of magnitude lower than the PCASP. Additional measurements of aerosol size distributions from 15 min of SLR during the same flight at 30 m ASL over oceans suggest that sea-salt aerosol is detected and sized reasonably by the FFSSP. A possible reason for the behavior of the FFSSP is that the supermicron regional haze aerosol particles may not be spherical. This assertion is examined using results from the SID probe during the same SLRs. Experience with the SID probe in ice/mixed phase is used to define a SID asphericity factor (SAF) of unity as the interface between spherical and nonspherical scattering [*Hirst et al.*, 2001]. Normalized values are plotted in Figure 6, so that SAFs greater than 1 represent increasingly nonspherical scattering, and less than 1 indicates spherical scattering behavior. Figure 6a shows that supermicron aged regional haze particles typically have a SAF exceeding this threshold (mean SAF 1.84) and therefore the majority (75% in this case) of the particles are nonspherical. Figure 6b shows that sea-salt aerosol is almost universally spherical (mean SAF 0.57). Note however that in this case, the SAF shows a degree of bimodality. The most likely explanation is that some of the aerosol is mixing down to the surface. This suggests that the aged regional haze mixes down into the marine boundary layer over ocean and may thus interact with Sc cloud leading to changes in the microphysical and radiative properties of clouds. By themselves, these results do not explain the discrepancy between the PCASP and the FFSSP size distributions in the $1-2$ μm range because one might expect a reduction in detection rate by the FFSSP of up to a factor of 4 (25% of the supermicron particles are spherical). However, Figure 7 shows a discrep-

Table 1. The Midpoint Radius (μm) of the PCASP-100X Instrument When Calibrated With Latex Spheres ($n = 1.585 - 0i$) and the Computed Midpoint Assuming the Refractive Indices of Aged Biomass Aerosol Particles $(1.54 - 0.018i)$[a]

PCASP Bin Number	Midpoint ($n = 1.585 - 0i$) (μm)	Midpoint ($n = 1.54 - 0.018i$) (μm)	$r_{aerosol}/r_{latex}$	Contribution to Scattering at 0.55 μm (%)
1	0.0550	0.0674	0.81	0.2
2	0.0650	0.0760	0.85	0.4
3	0.0775	0.0871	0.88	1.2
4	0.0925	0.1007	0.91	2.8
5	0.1125	0.1199	0.93	10.4
6	0.1375	0.1450	0.94	25.8
7	0.1750	0.1852	0.94	41.6
8	0.2250	0.2393	0.93	9.4
9	0.3000	0.3219	0.93	2.4
10	0.4000	0.4292	0.93	1.1
11	0.5250	0.8246	0.63	0.8
12	0.6750	1.1593	0.58	0.4
13	0.8750	1.1768	0.74	1.2
14	1.1250	2.0400	0.55	1.3
15	1.3750	2.9910	0.45	1.0

[a]The fractional error $r_{aerosol}/r_{latex}$ shows that the PCASP will tend to underestimate the size of biomass aerosol particles due to the effects of particulate absorption. The contribution to the total scattering at 0.55μm is calculated using Mie scattering theory and the mean aerosol size distribution shown in Figure 7. Bins $4-10$ contribute over 93% of the aerosol scattering and absorption at 0.55 μm.
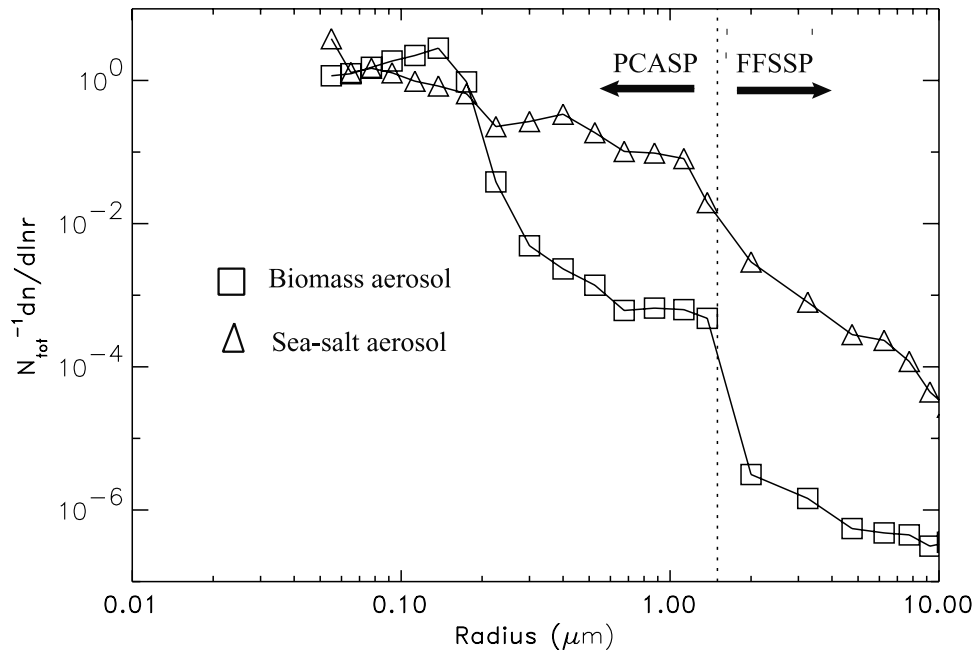
Figure 5. An example of the discontinuity between the aerosol PCASP and the FFSSP size distributions. For comparison, a hydrated sea-salt aerosol size distribution size distribution is also shown, which does not show a discontinuity at 1.3 μm.

ancy between the PCASP and the FFSSP concentrations between 1 and 2 μm of 2 orders of magnitude, and thus nonsphericity alone is unlikely to account for the discrepancy. The FSSPs on the South African Aerocommander aircraft were subject to similar detection problems (S. Piketh, personal communication, 2002). Because of the uncertainties in the size distributions determined by the FFSSP, we restrict further analyses to using the PCASP size distributions.

6.3. Results

[21] The average normalized number ($dN/dlnr$) and normalized volume distributions ($dV/dlnr$) obtained for each flight during the campaign from the PCASP probe are shown in Figures 7a and 7b. The similarity of the shape of the aged aerosol size distribution throughout the campaign is clearly evident. Figure 7a shows that the aged aerosol number distribution shows evidence of a mode between 0.1 and 0.2 μm radius The fresh biomass smoke from the Otavi plume shows a significantly different aerosol size distribution with higher concentrations of small Aitken mode particles. Figure 7b shows the same measurements plotted as volume distributions. Again the fresh Otavi plume aerosol shows significantly larger aerosol volume (or equivalently aerosol mass) at smaller sizes. Besides the dedicated flights, aged regional haze was also sampled during a profile ascent from Ascension Island (8°S, 14°W) on flight a794 on 19 September 2000 while the C-130 was en route back to the UK. Evidence that this was aged regional haze originating in southern Africa comes from back-trajectory analysis that indicates the aerosol crossed the coast of Angola some 5 days previously, and from TOMS imagery that clearly shows the aerosol being transported such distances (e.g., Figure 2). Particles larger than 0.6 μm radius are entirely absent in these measurements. The mean number distribution may be fitted throughout the

optically active 0.1–1.0 μm radius range by using a minimum of two or three lognormal distributions of the form:

$$\frac{dn_i(r)}{d \ln r} = \frac{n_i}{\sqrt{2\pi}} \frac{1}{\ln \sigma} \exp\left[\frac{-(\ln r_i - \ln r_n)^2}{2(\ln \sigma)^2}\right] \quad (3)$$

where $dn_i(r)$ is the number of particles in the range r to $r + dlnr$, and r_n and σ are the geometric mean radii and standard deviations. Two or three lognormal distributions
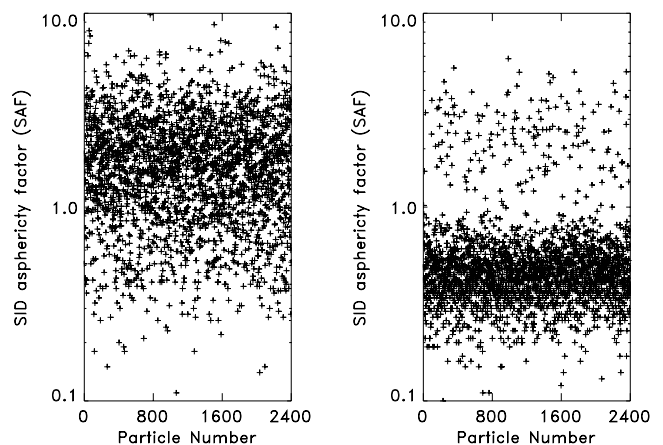

Figure 6. The SAF for SLRs during flight a789 on 11 September 2000. (a) The SAF for aged regional haze aerosol from a SLR performed at 2620 m ASL (750 hPa). (b) The SAF for sea-salt aerosol from a SLR performed at 32 m ASL. Values above unity indicate that the scattering from the aerosol is typical of nonspherical particles.
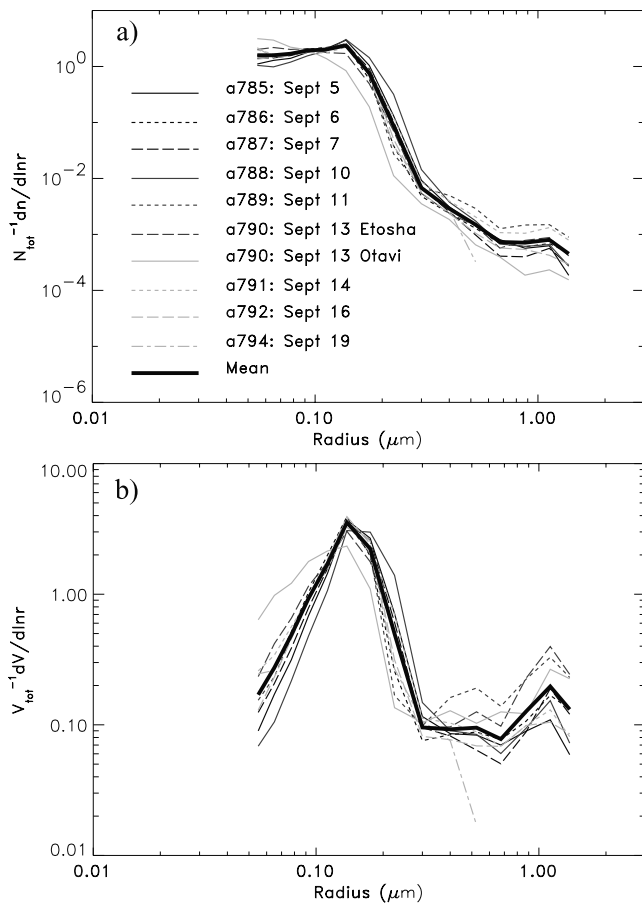
Figure 7. The normalized flight mean number and volume distributions of the aerosol measured during SAFARI 2000. The locations of the flights are shown in Figure 1. The mean distribution is a mean from all the composite distributions excluding data from the Otavi plume and from the measurements in Ascension Island. a790 Etosha indicates measurements made in aged haze over the Etosha Pan, while a790 Otavi indicates measurements made in a fresh plume described in the text. The Ascension Island measurements (a794) were taken outside of the region shown in Figure 1 during a transit flight returning to the UK.

are used here because this is the minimum number of lognormal modes that adequately represents the particle size distributions. More modes could be used to improve the fit further, but this would limit their usefulness to the scientific community. A basic fit was performed initially, then the number faction, r_n and σ of each mode were varied about the initial values. The best fit was considered to be the combination of number faction, r_n and that minimized the difference between the total scattering computed using the measured and fitted size distributions. Table 1 shows that ~95% of the scattering at 0.55 μm is represented by the particles between 0.0925 and 0.4 μm. Thus it is important to fit bin number 7 the most accurately, bin 6 the second most accurately, etc. This method of performing the fits is not intended as a radiative closure test, merely to ensure that the optical parameters calculated from the lognormal distributions best represent the measured aerosol

size distributions and their associated optical properties. Figure 8 shows the three lognormal distributions used and resultant fit with Table 2 showing r_n and σ for each mode for aged aerosol, for aerosol in the Otavi plume, and for the aerosol measured off Ascension Island.

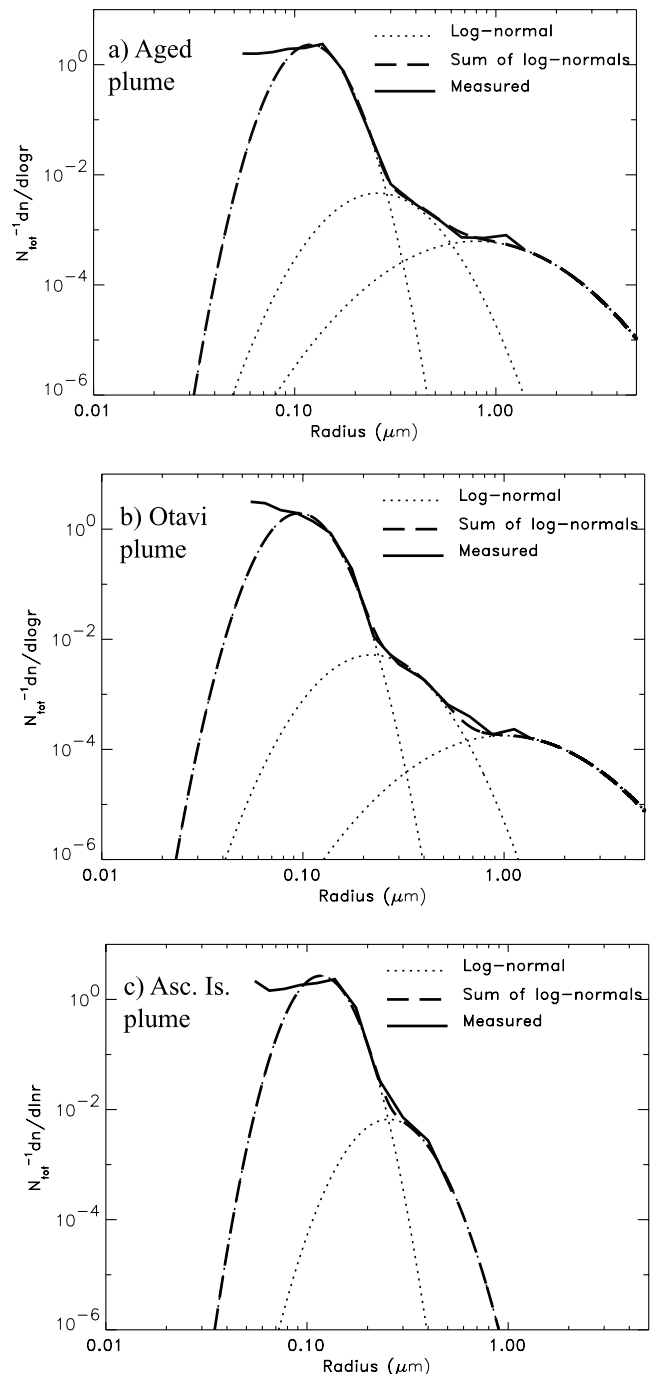**Figure 8.** The normalized size distribution fitted by summing three lognormal distributions. The geometric mean and standard deviations of the lognormal distributions are given in Table 3 together with the calculated optical parameters. (a) Aged plume, labeled "mean" in Figure 7, (b) fresh Otavi plume, labeled "a790 13 September: Otavi" in Figure 7, and (c) very aged plume over Ascension Island, labeled "a794" in Figure 7.

Table 2. The Flight Mean Optical Properties of Aged Regional Haze[a]

Flight Number and Date	N_{tot} (cm^{-3})	Volume Fraction/ Particle	Derived from PCASP									Derived From Nephelometer and PSAP		
			g			ω_o			k_e (m^2 g^{-1})			ω_o		
			$\lambda = 0.45$	$\lambda = 0.55$	$\lambda = 0.70$	$\lambda = 0.45$	$\lambda = 0.55$	$\lambda = 0.70$	$\lambda = 0.45$	$\lambda = 0.55$	$\lambda = 0.70$	$\lambda = 0.45$	$\lambda = 0.55$	$\lambda = 0.70$
a785: 5 September	1174	9.20×10^{-21}	0.65	**0.59**	0.50	0.91	**0.90**	0.89	6.7	**4.7**	2.8	0.88	**0.87**	0.84
a786: 6 September	899	7.55×10^{-21}	0.63	**0.56**	0.47	0.92	**0.89**	0.87	5.8	**4.0**	2.3	0.87	**0.86**	0.83
a787: 7 September	1786	8.41×10^{-21}	0.64	**0.58**	0.50	0.91	**0.90**	0.88	6.5	**4.6**	2.7	0.94	**0.93**	0.91
a788: 10 September	1570	1.131×10^{-20}	0.66	**0.61**	0.53	0.92	**0.91**	0.89	7.0	**5.1**	3.1	0.93	**0.92**	0.90
a789: 11 September	974	8.84×10^{-21}	0.64	**0.58**	0.50	0.90	**0.89**	0.86	5.6	**3.9**	2.4	0.87	**0.86**	0.84
a790 Etosha: 13 September	2862	6.67×10^{-21}	0.62	**0.57**	0.49	0.92	**0.88**	0.86	5.4	**3.8**	2.3	0.89	**0.87**	0.84
a790 Otavi: 13 September	*31091*	*4.223×10^{-21}*	*0.59*	*0.52*	*0.43*	*0.86*	*0.84*	*0.81*	*5.2*	*3.5*	*2.1*	*0.86*	*0.84*	*0.80*
a791: 14 September	744	9.59×10^{-20}	0.65	**0.60**	0.52	0.91	**0.90**	0.88	6.4	**4.6**	2.8	0.92	**0.91**	0.89
a792: 16 September	1298	7.84×10^{-21}	0.64	**0.57**	0.48	0.91	**0.90**	0.88	6.3	**4.4**	2.6	0.93	**0.92**	0.91
a794 Ascension Island: 19 September	305	7.15×10^{-21}	0.63	**0.57**	0.48	0.91	**0.90**	0.88	6.3	**4.3**	2.5	n/a	n/a	n/a
Mean from Figure	1070	7.97×10^{-21}	0.64	**0.58**	0.50	0.91	**0.90**	0.88	6.1	**4.3**	2.6	0.91	**0.90**	0.87

[a]The optical parameters derived from the PMS probes assume a wavelength-dependent real refractive index determined from the chemical composition to be $1.54 - 0.018i$. The ω_o, derived from the PSAP and nephelometer applies the corrections described by *Bond et al.* [1999] and by *Anderson and Ogren* [1998]. Optical parameters at 0.55 μm are highlighted in bold. Italics are used to highlight measurements in the fresh biomass burning plume detected over Otavi, which significantly different size distributions and optical parameters. An imaginary refractive index of $0.025i$ is used in the calculations for the Otavi plume. The mean optical properties in the last row are calculated from the mean size distribution shown in Figure 7. Note that the k_e quoted here are over the range of size distributions measured by the PCASP. The lognormal distributions provide more reasonable estimates, as they contain all of the aerosol mass.

[22] For the aged plume, fits to the data for each of the flights reveals that r_n and σ for modes 1 and 2 differ by less than ±0.01 and ±0.1 respectively from the means shown in Table 1, and these values are therefore used as estimates of the error. The number fraction from mode 1 ranges from 0.9950 to 0.9997. For the largest mode, r_n differs by less than ±0.01, but there are significant differences in σ, due to the large particle size distribution being poorly constrained by the PCASP.

[23] Size distributions from Ascension Island (8°S, 14°W) on 19 September 2000 reveal a similar fit to the first two modes, while mode 3 is missing. This indicates that while the large dust mode is removed (probably by sedimentation), the size distribution of the optically active size particles does not change significantly even when transported more than 2500 km from the coast of Angola.

[24] The fresh Otavi plume has a smaller r_n for both mode 1 and mode 2 while σ is the same for both modes. These lognormal distributions may prove useful for modeling studies that initially produce biomass aerosol as a fresh mode that subsequently ages.

7. Aerosol Optical Parameters

[25] Three methods for determining the optical parameters are investigated here. The first uses PCASP measurements of the size distributions of aerosols together with the refractive indices determined in section 5 and Mie scattering theory. The second uses lognormal fits to the mean size distribution, and the third provides independent measurements of the scattering and absorption coefficients with the PSAP and nephelometer.

7.1. Determination of the Optical Properties From In Situ Measurements of the Size Distribution and Assumed Refractive Indices

[26] The optical properties of the aerosol size distributions shown in Figures 7a and 7b are determined using Mie scattering theory and the refractive indices determined from the chemical composition. As in section 5, the effects of relative humidity are neglected. The results are summarized in Table 2.

[27] For the aged plume, the specific extinction coefficient at a wavelength of 0.55 μm, $k_{e\lambda=0.55}$, ranges from 3.8 to 5.1 m^2 g^{-1} while the asymmetry factor, $g_{\lambda=0.55}$, ranges from 0.56 to 0.61, and the single scattering albedo, $\omega_{o\lambda=0.55}$, is in the narrow range 0.89–0.91. The mean optical parameters at 0.55 μm determined from the mean size distribution are $k_{e\lambda=0.55} = 4.3$ m^2 g^{-1}, $g_{\lambda=0.55} = 0.58$, and $\omega_{o\lambda=0.55} = 0.90$. To estimate the approximate error that may be introduced by neglecting differences in refractive index between the aerosol and the calibration spheres (section 6.1), the PCASP midpoint radii for aged regional haze were also used in the calculations for the mean size distribution. The results yield $k_{e\lambda=0.55} = 3.1$ m^2 g^{-1}, $g_{\lambda=0.55} = 0.59$, and $\omega_{o\lambda=0.55} = 0.89$. Thus the neglect of this factor leads to differences in $\omega_{o\lambda=0.55}$ and $g_{\lambda=0.55}$ of less than 2%, but a 25% error in the computed $k_{e\lambda=0.55}$.

[28] For the Otavi plume, a refractive index of $1.54 - 0.025i$ is used which is consistent with measurements by the PSAP and nephelometer (section 7.3). This value of refractive index indicates more absorption, and use of the Maxwell-Garnet mixing rule suggests a $M_{ECa/total}$ of

Table 3. The Geometric Mean Radii (r_n) and Standard Deviations (σ) for the Three Lognormal Number Distributions[a]

	Mode	Aerosol Type	Number Fraction	$r_n \pm 0.01$ (μm)	$\sigma \pm 0.1$[b]	$k_{e\lambda=0.55\ \mu m}$ ($m^2\ g^{-1}$)	$\omega_{o\lambda=0.55\ \mu m}$	$g_{\lambda=0.55\ \mu m}$
Aged	1	Biomass	0.9960	0.12	1.30	5.06	0.91	0.59
	2	Biomass	0.0033	0.26	1.50	4.56	0.89	0.71
	3	Dust	0.0007	0.80	1.90	0.29	0.77	0.81
	1 + 2	**Biomass**	**N/A**	**N/A**	**N/A**	**5.04**	**0.91**	**0.59**
	1 + 2 + 3	Biomass + Dust	N/A	N/A	N/A	2.14	0.90	0.61
Fresh Otavi	1	Biomass	0.9957	0.10	1.30	4.01	0.86	0.51
	2	Biomass	0.0041	0.22	1.50	1.49	0.87	0.72
	3	Dust	0.0002	1.00	1.90	0.12	0.68	0.87
	1 + 2	**Biomass**	**N/A**	**N/A**	**N/A**	**3.86**	**0.86**	**0.52**
	1 + 2 + 3	Biomass + Dust	N/A	N/A	N/A	0.72	0.70	0.57
Aged Ascension Island	1	Biomass	0.9997	0.117	1.25	4.54	0.90	0.55
	2	Biomass	0.0003	0.255	1.4	5.56	0.90	0.71
	1 + 2	**Biomass**	**N/A**	**N/A**	**N/A**	**4.54**	**0.90**	**0.55**

[a]For modes 1 and 2, the optical parameters at 0.55 μm are calculated using a density of 1.35 g cm^{-3} and $n_{eff} = 1.54 - 0.018i$ for the aged plumes and 1.54 $-$ 0.025i for the fresh Otavi plume. For mode 3, a density of 2.65 g cm^{-3} and n_{eff} of 1.53 $-$ 0.008i is assumed [*WCP*, 1986].
[b]For mode 3, the estimate of the error in σ is 0.4.

approximately 0.075 for fresh biomass burning aerosol. $k_{e\lambda=0.55}$ is calculated to be 3.4 m^2 g^{-1}, while $g_{\lambda=0.55}$, is 0.51, and $\omega_{o\lambda=0.55}$ is 0.84. The smaller $k_{e\lambda=0.55}$ and $g_{\lambda=0.55}$ than for the aged plume are indicative of smaller particles. Further calculations were performed using refractive indices of 1.54 $-$ 0.018i (i.e., the refractive indices typical of the aged plume). The results show that the derived $\omega_{o\lambda=0.55}$ is 0.88 when an imaginary refractive index 0.018i is used, which does not compare as well to the $\omega_{o\lambda=0.55}$ measured by the PSAP and nephelometer (section 7.3).

7.2. Determination of the Optical Properties Using Lognormal Distributions

[29] Aerosol optical parameters may also be calculated for each of the three modes described in section 6.3 using Mie scattering theory for aged regional haze and fresh biomass aerosol. For the smallest two modes, the refractive index at 0.55 μm is assumed to be 1.54 $-$ 0.018i for aged aerosol and 1.54 $-$ 0.025i for the Otavi plume. The density of the aerosol is assumed to be 1.35 g cm^{-3} [*Reid and Hobbs*, 1998]. The third mode is likely to contain a significant amount of dust (supported by the filter measurements in the coarse fraction, [*Formenti et al.*, 2003]) and so the refractive indices of dust-like aerosol are used together with a density of 2.65 g cm^{-3} [*WCP*, 1986]. ω_o, g, and k_e, for each of the modes may then be calculated as a function of wavelength. Table 3 shows these optical parameters at a wavelength of 0.55 μm. Note that *Sokolik and Toon* [1996] present imaginary refractive indices for different types of mineral dust that vary by a factor of 3. Calculations that assume an imaginary part of the refractive index of 1.53 $-$ 0.0015i [*Haywood et al.*, 2003b] for mineral dust result in $\omega_{o\lambda=0.55} = 0.93$ for the dust mode for the aged aerosol rather than 0.77 indicating the large degree of uncertainty associated with estimating the absorption and $\omega_{o\lambda}$ for the dust mode. The optical parameters may also be calculated for the sum of the lognormal distributions as shown in Table 3. These lognormal distributions and optical parameters may be used in GCM studies investigating the radiative forcing due to biomass burning aerosol [e.g., *Myhre et al.*, 2003]. Note that k_e obtained by summing the three lognormal distributions are lower than those shown in Table 2. This is because the use of lognormal distributions includes all the aerosol mass while the PCASP

instrument detects the optically active particles, but does not detect the significant amount of aerosol mass outside the PCASP size range (particularly the larger particles). It is therefore best practice to use specific coefficients derived from lognormal distributions.

7.3. Determination of the Optical Properties From In Situ Measurements With the Nephelometer and PSAP

[30] Measurements were performed using the PSAP and nephelometer over periods identical to those used in calculating the PCASP mean aerosol size distributions shown in Figure 9. The nephelometer was corrected for variations from Standard Temperature and Pressure (STP), for truncation of the scattered radiation between scattering angles of approximately 7°–170° and for deficiencies in the illumination source [*Anderson and Ogren*, 1998]. The PSAP was corrected for variations in the area of the exposed filter, inaccuracies in the flow rate measured by the instrument, for scattering being misinterpreted as absorption, and for multi-
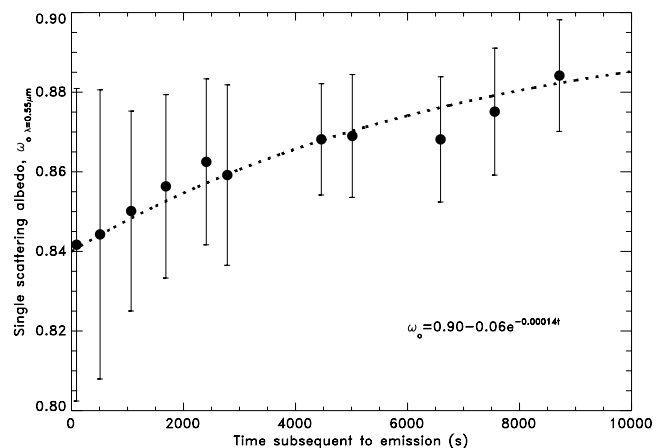

Figure 9. $\omega_{o\lambda=0.55\mu m}$ measured by the PSAP and nephelometer as a function of time subsequent to emission from the Otavi source. The time from emission is estimated from the mean components of the measured wind speed. The error bars represent one standard deviation in the measurements.
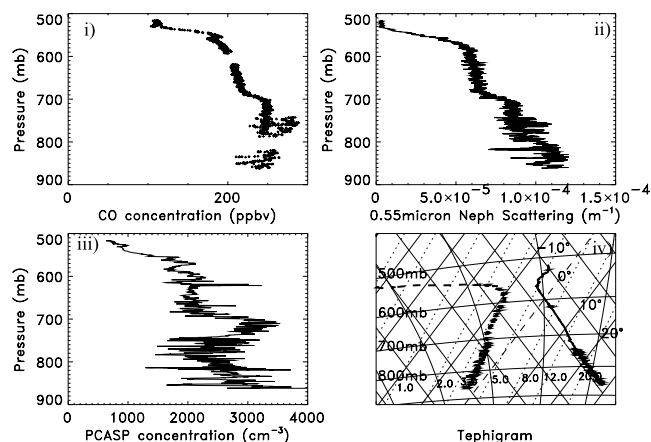
Figure 10. Profiles of (1) CO (ppbv), (2) 0.55 μm nephelometer σ_{sca}, (3) PCASP number concentration (cm^{-3}), and (4) T, T$_d$ (K) on a standard tephigram. Data are from a profile down to 16 m at 1205 local time. The aerosol is mixed down to the surface due to the onset of convection in the dry convective boundary layer, which extends from the surface to approximately 550 hPa (5000 m ASL). The correlation between CO, aerosol scattering, and aerosol concentration is evident.

ple scattering [*Bond et al.*, 1999]. Both of these sets of corrections tend to decrease the absorption coefficient and increase the scattering coefficient, hence raising $\omega_{o\lambda}$ [see *Haywood and Osborne*, 2000]. While the nephelometer measures at three wavelengths (0.45, 0.55, and 0.70 μm), the PSAP measures the absorption at 0.567 μm. This enables determination of $\omega_{o\lambda=0.55}$, but assumptions have to be made about the wavelength dependence of the absorption coefficient to enable estimation of $\omega_{o\lambda=0.45}$ and $\omega_{o\lambda=0.70}$. Here we make the assumption that the absorption coefficient is proportional to $1/\lambda$ [*Reid and Hobbs*, 1998]. The model calculations with a fixed imaginary part of the refractive index of 0.018i suggest this is a more realistic assumption than a wavelength independent absorption coefficient. The results are summarized in the last column of Table 2.

[31] Values of $\omega_{o\lambda}$ from the PSAP and nephelometer are in reasonable agreement overall with $\omega_{o\lambda}$ derived from PCASP measurements of the size distribution when imaginary refractive indices of 0.018i for aged aerosol and 0.025i for fresh aerosol in the Otavi plume are used in the Mie scattering calculations. The PSAP and nephelometer measurements were also examined as the aircraft operated at constant altitude in a raster pattern further down the Otavi plume. The time from emission source was estimated using the mean northerly and westerly wind speeds measured by the C-130. Figure 9 shows that the difference in $\omega_{o\lambda=0.55}$ is statistically significant (to 1 standard deviation) when comparing that measured at source to that measured further down the plume.

[32] A simple exponential fit of the form,

$$\omega_{o\lambda=0.55} = 0.90 - 0.06\exp -0.00014t, \qquad (4)$$

where t is the time in seconds, is fitted to the data and included in Figure 9. This shows that $\omega_{o\lambda=0.55}$ tends to increase with time indicating that the aerosol becomes less

absorbing as it ages. This finding is discussed in more detail in section 9.

8. Vertical Profiles of CO and Aerosol Concentrations and Scattering

[33] The vertical distribution of aerosols has been shown to be extremely important in determining the magnitude and even the sign of the radiative effect, particularly in the presence of cloud. Using realistic cloud and aerosol optical properties and vertical profiles measured during SAFARI 2000, *Keil and Haywood* [2003] show that the strong negative radiative effect (i.e., an increase in local planetary albedo) of the biomass-rich aerosol in cloud-free conditions is modified to become strongly positive (i.e., a decrease in planetary albedo) when the aerosol exists above highly reflecting Sc cloud. Therefore examples of typical vertical profiles of aerosol scattering and concentration over land and over ocean are presented here together with corresponding tephigrams and CO concentrations.

[34] Within the aged regional haze, aerosol number concentration, nephelometer scattering coefficients, and carbon monoxide concentrations were found to be well correlated. *Formenti et al.* [2003] present a full analysis of the correlation coefficients between these variables. Examples of these three parameters are shown over land (Figure 10) and over ocean (Figure 11).

[35] Figure 10 shows the vertical profile of CO (ppbv), the 0.55 μm scattering coefficient (m^{-1}), and PCASP number concentration (cm^{-3}) to an altitude of 16 m on 13 September 2000 at 1205 local time. At 0800 GMT (1000 local time) the nocturnal boundary layer, which had been observed on takeoff, had broken down in response to the strong solar surface heating. Consequently, the aerosol is
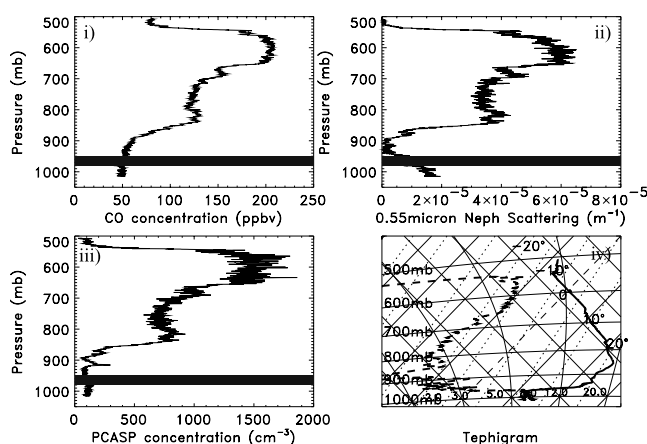

Figure 11. Profiles of (1) CO (ppbv), (2) 0.55 μm nephelometer σ_{sca}, (3) PCASP number concentration (cm^{-3}), and (4) T and T$_d$ (K) on a standard tephigram. Data are from a profile off the coast of Namibia on 11 September 2000. The main aerosol layer lies between 550 and 650 hPa (3000–5000 m ASL) although elevated aerosol layers exist down to 850 hPa (2000 m ASL). The correlation between CO, aerosol scattering, and aerosol concentration is evident. The shaded area in (1)–(3) represents the vertical extent of stratocumulus cloud.

relatively well mixed down to the surface with the tephigram showing a temperature profile close to the dry adiabatic lapse rate. The correlation between CO, particle concentration, and particle scattering is clearly evident.

[36] Figure 11 shows profiles of CO, aerosol scattering coefficient and aerosol number concentration over the ocean from flight a789 on 11 September. The main aerosol layer lies between 850 and 500 hPa (3000–5000 m ASL) with elevated aerosol concentrations down to 900 hPa (1500 m). Below this altitude, there is a distinct "clean slot" where the aerosol concentrations, the aerosol scattering, and the CO concentrations are reduced to pristine conditions above the Sc cloud which is capped by a strong (>10 K) inversion. Analysis of further profiles from this flight reveals that the lowermost extent of the aerosol is variable with one profile indicating significant aged regional haze aerosol and CO at 950 hPa, indicating that interaction of aerosol and Sc cloud is likely to occur.

[37] The mean altitude of the top of the aerosol layer was determined from 31 profiles (over land and ocean) of nephelometer scattering to be approximately 4900 m ASL with a standard deviation of 700 m. The mean altitude of the bottom of the aerosol layer was determined from 27 nephelometer profiles (over ocean only as the aerosol became well mixed vertically during the day, over land, see Figure 10) to be 1500 m with a standard deviation of 600 m.

9. Discussion and Conclusions

[38] The chemical composition analysis suggests that for particle size <0.65 μm radius (i.e., the particle size class most optically active in the solar spectrum), the ratio of EC_a mass to OC mass, $M_{ECa/OC}$, is approximately 0.12 for aged aerosol. These results are similar to the results of Ferek et al. [1998] who reported $M_{ECa/OC}$ of 0.08 (smoldering combustion) to 0.12 (all fires) in Brazil during the Smoke, Clouds and Radiation-Brazil (SCAR-B) experiment. Ruellan et al. [1999] also reported similar $M_{ECa/OC}$ ratios of 0.08 (smoldering combustion) and 0.11 (flaming combustion) in Southern Africa. These results are obtained using similar thermal optical techniques to that presented here and taken together, the results suggest that $M_{ECa/OC}$ is relatively invariant between biomass burning regions, which is encouraging for global modeling efforts that need to make simplifying assumptions. Ferek et al. [1998] suggested that approximately 10% of the total aerosol mass is composed of inorganic compounds, whereas the results presented here suggest a higher fraction of inorganic material at approximately 25%. Possible reasons for these differences include different vegetation, soil, and burning practices. In particular, we have found that smoke from deforestation fires in Amazonia contains very little resuspended soil dust, in contrast to smoke from African savanna fires [Andreae et al., 2002, and references therein].

[39] By applying reasonable assumptions about the refractive indices and density of EC_a and OC, a refractive index of $1.54 - 0.018i$ is deduced at a wavelength of 0.55 μm for aged aerosol and $1.54 - 0.025i$ for fresh aerosol. Both volume weighting the refractive indices and the Maxwell-Garnet mixing rule are used in this study, and both are found to be suitable for determining the refractive indices, providing a density of EC of 1.7 g

cm^{-3} is used. Ross et al. [1998] assume a similar density of 1.8 g cm^{-3} for EC in their study of young biomass burning particles in Brazil. Similar real and imaginary parts of the refractive index are found in analysis of the CIMEL data from the Etosha site in northern Namibia [Haywood et al., 2003a], which supports the use of these refractive indices.

[40] The size distributions of the aged aerosol are remarkably similar to each other, considering that the measurements were performed over an 11-day time period and over a wide geographical region. C-130 measurements of the PCASP size distributions of industrial pollution during the Tropospheric Aerosol Radiative Forcing Observational Experiment (TARFOX) [e.g., Francis et al., 1999], and during the Aerosol Characterization Experiment-2 (ACE-2) [e.g., Johnson et al., 2001] show much greater day-to-day variability. Three lognormal distributions are shown to adequately characterize the aerosol size distribution in the optically important 0.1–1.0 μm radius range. For aged aerosol r_n are 0.12 ± 0.01, 0.26 ± 0.01, and 0.80 ± 0.30 μm and σ are 1.3 ± 0.1, 1.5 ± 0.1, and 1.9 ± 0.1 for each of the three modes. For fresh aerosol in the Otavi plume, r_n are 0.10, 0.22, and 1.00 μm and σ are 1.3, 1.5, and 1.9 for each of the three modes. For the very aged aerosol measured off Ascension Island, a distance of over 2500 km from the coast of Namibia, the large dust mode has disappeared presumably as a result of sedimentation. Of these aerosol modes, mode 1 adequately describes the optical properties at 0.55 μm, results that may prove useful in global modeling efforts.

[41] $\omega_{o\lambda=0.55\mu m}$, computed from the PCASP measured size distribution and the computed refractive indices, have a mean of 0.90 for aged aerosol and 0.84 for fresh aerosol in the Otavi plume. These calculations are relatively insensitive (<2% difference) to whether corrections are applied to the PCASP size distributions based on the difference in refractive index between the aerosol and the calibrating spheres. The measurements of the aged aerosol are in agreement with $\omega_{o\lambda=0.55\mu m}$ derived from independent measurements of aerosol scattering and absorption made with the nephelometer and the PSAP. Measurements of the monthly mean ω_o using the Dubovik et al. [2000] retrieval algorithm from the Etosha AERONET site [Holben et al., 1998] suggest $\omega_{o\lambda=0.44\mu m}$ of 0.92 (SD 0.04) and $\omega_{o\lambda=0.67\mu m}$ of 0.91 (SD 0.04), which are consistent with the aircraft measurements. Eck et al. [2001] deduced a $\omega_{o\lambda=0.55\mu m}$ of 0.84 ± 0.03 for biomass aerosol in Zambia, which is indicative of a somewhat more absorbing aerosol than the aged aerosol measured here. A possible cause of this lower $\omega_{o\lambda=0.55\mu m}$ is that the CIMELS sites in Zambia are much closer to the local sources and the aerosol is therefore less aged. Our lower value of $\omega_{o\lambda=0.55\mu m}$ of 0.84 for fresh aerosol in the Otavi plume supports this hypothesis. Penner et al. [2001] state a central value of $\omega_{o\lambda=0.55}$ of 0.89 for biomass aerosol, which is also in agreement with the measurements presented here. Hobbs et al. [1997] and Reid et al. [1998b] report a $\omega_{o\lambda=0.55}$ of 0.83 for biomass aerosol in Brazil, which is significantly lower than that presented here. Reasons for these differences are unclear.

[42] $\omega_{o\lambda=0.55\mu m}$ measured by the PSAP and nephelometer as the plume ages suggests less absorption as the plume ages which may indicate condensation of OC onto the aerosol particles.

[43]   To estimate the error in $\omega_{o\lambda=0.55}$ for the aged regional haze, the standard deviation from the measurements made by the nephelometer and PSAP shown in Table 2 is computed. The estimate of ±0.03 (±1 standard deviation) includes variability in the chemical composition of the aerosol that is not included in the computations of $\omega_{o\lambda=0.55}$ from the size distributions measured by the PCASP, which assume a fixed refractive index (also included in Table 2). However, there are likely additional systematic errors associated with the corrections applied to the nephelometer scattering and PSAP absorption (section 7.3). Following the error analysis of *Haywood and Osborne* [2000], we estimate an additional random error of ±0.02. Root mean square error analysis suggests $\omega_{o\lambda=0.55} = 0.91 \pm 0.04$ appears a reasonable assessment.

[44]   The range in the specific extinction coefficient, $k_{e\lambda=0.55}$, should be computed from lognormal distributions because the PCASP detects the optically active particles, but not all of the aerosol mass. Unlike the error assessment of $\omega_{o\lambda=0.55}$, there are no independent measurements of $k_{e\lambda=0.55}$ and therefore the standard deviation derived from Mie calculations derived from the PCASP size distribution is computed. In computing the standard deviation, the PCASP size distribution was truncated at bin 12 (0.675 μm) to exclude the influence from mineral dust and Mie scattering theory was then used to determine $k_{e\lambda=0.55}$ for the truncated size distributions. The standard deviation computed in this way was 0.6 m^2 g^{-1}. Correcting the PCASP radii for differences in the refractive index between the calibrating spheres and the aerosol leads to additional potential errors much smaller than the 25% calculated in section 7.1 because of the removal of the large particles where the sizing is most uncertain (Table 1) and is estimated as ±0.2 m^2 g^{-1}. Thus $k_{e\lambda=0.55} = 5.0 \pm 0.8$ m^2 g^{-1} is estimated for aged aerosol if lognormal modes 1 and 2 are considered. *Reid et al.* [1998b] also remove the mineral dust/soil contribution from their measurements of aged regional haze in during SCAR-B, and determines $k_{e\lambda=0.55}$ as 4.8 ± 1.0 m^2 g^{-1} which is in agreement with our calculations. *Formenti et al.* [2003] derived the specific scattering coefficient, $k_{s\lambda=0.55}$, using two different sets of assumptions by correlating the nephelometer scattering coefficient to the submicron aerosol mass from the PCASP and found $k_{s\lambda=0.55}$ of 4.2 ± 0.8 and 4.6 ± 0.6 m^2 g^{-1}. Division by $\omega_{o\lambda=0.55}$ of 0.91 leads to values of $k_{e\lambda=0.55}$ that are entirely in agreement with our estimates.

[45]   The uncertainty in $g_{\lambda=0.55}$ is determined in a similar way to $k_{e\lambda=0.55}$. From the lognormal size distributions $g_{\lambda=0.55} = 0.59 \pm 0.02$ appears reasonable. The estimate of $g_{\lambda=0.45}$ of 0.64 ± 0.02 from the measured size distribution is in agreement with the $g_{\lambda=0.44}$ of 0.65 derived by *Remer et al.* [1998] for South American biomass smoke during SCAR-B.

[46]   These measurements also suggest that modeling studies could use a single lognormal distribution with a r_n of 0.12 μm and σ of 1.3 to adequately represent the optical properties of aged regional haze without a significant loss in accuracy.

[47]   Measurements of the vertical profile of the aerosol are particularly important for partially absorbing aerosols, as absorbing aerosols existing above highly reflective surfaces such as the Sc sheet may give a positive rather than a negative radiative effect [e.g., *Keil and Haywood*, 2003]. The measurements suggest that the aged regional haze frequently exists above the Sc and that the interaction of Sc and aerosol is often limited by the temperature inversion capping the cloud.

[48]   While these measurements are representative of aged regional haze well downwind of areas of extensive biomass burning in southern Africa during September, there is some evidence that suggests the degree of absorption of the aerosol may change throughout the burning season [*Eck et al.*, 2003]. Additionally, the majority of the burning sampled here is from burning of savanna grasses/cerrado for soil fertilization purposes. Biomass aerosol from deforestation will likely have significantly different optical properties. Further studies at regional scales are required to address these issues.

References

Anderson, T. L., and J. A. Ogren, Determining aerosol radiative properties using the TSI 3563 integrating nephelometer, *Aerosol Sci. Technol.*, 29, 57–69, 1998.

Andreae, M. O., W. Elbert, R. Gabriel, D. W. Johnson, S. Osborne, and R. Wood, Soluble ion chemistry of the atmospheric aerosol and SO$_2$ concentrations over the eastern North Atlantic during ACE-2, *Tellus*, 52B, 1066–1087, 2000.

Andreae, M. O., et al., Biogeochemical cycling of carbon, water, energy, trace gases and aerosols in Amazonia: The LBA-EUSTACH experiments, *J. Geophys. Res.*, 107(D20), 8066, doi:10.1029/2001JD000524, 2002.

Birch, M. E., and R. A. Cary, Elemental carbon-based method for monitoring occupational exposures to particulate diesel exhaust, *Aerosol Sci. Technol.*, 25, 221–241, 1996.

Bond, T. C., T. L. Anderson, and D. Campbell, Calibration and intercomparison of filter-based measurements of visible light absorption by aerosols, *Aerosol Sci. Technol.*, 30, 582–600, 1999.

Chýlek, P., V. Srivastava, R. G. Pinnick, and R. T. Wang, Scattering of electromagnetic waves by composite spherical particles: Experiment and effective medium approximations, *Appl. Opt.*, 27, 2396–2404, 1988.

Chow, J. C., J. G. Watson, D. Crow, D. H. Lowenthal, and T. Merrifield, Comparison of IMPROVE and NIOSH carbon measurements, *Aerosol Sci. Technol.*, 34, 23–34, 2001.

Dubovik, O., A. Smirnov, B. N. Holben, M. King, Y. J. Kaufman, T. F. Eck, and I. Slutsker, Accuracy assessment of aerosol optical properties retrieval from AERONET sun and sky radiance measurements, *J. Geophys. Res.*, 105, 9791–9806, 2000.

Eck, T. F., B. N. Holben, D. E. Ward, O. Dubovik, J. S. Reid, A. Smirnov, M. M. Mukelabai, N. C. Hsu, N. T. O'Neill, and I. Slutsker, Characterisation of the optical properties of biomass burning aerosols in Zambia during the 1997 ZIBBEE field campaign, *J. Geophys. Res.*, 106, 3425–3448, 2001.

Eck, T., et al., Variability of biomass burning aerosol optical characteristics in southern Africa during the SAFARI 2000 dry season campaign and a comparison of single albedo estimates from radiometric measurements, *J. Geophys. Res.*, 108, doi:10.1029/2002JD002321, in press, 2003.

Ferek, R. J., J. S. Reid, P. V. Hobbs, D. R. Blake, and C. Liousse, Emission factors of hydrocarbons, halocarbons, trace gases and particles from biomass burning in Brazil, *J. Geophys. Res.*, 103, 32,107–32,118, 1998.

Francis, P. N., P. Hignett, and J. P. Taylor, Aircraft observations and modeling of sky radiance distributions from aerosol during TARFOX, *J. Geophys. Res.*, 104, 2309–2319, 1999.

Garvey, D. M., and R. G. Pinnick, Response characteristics of the particle measuring systems active scattering aerosol spectrometer probe (ASASP-X), *Aerosol Sci. Technol.*, 2, 477–488, 1983.

Haywood, J. M., and O. Boucher, Estimates of the direct and indirect radiative forcing due to tropospheric aerosols: A review, *Rev. Geophys.*, 38, 513–543, 2000.

Haywood, J. M., and S. R. Osborne, Corrections to be applied to the PSAP and nephelometer for accurate determination of the absorption

coefficient, scattering coefficient and single scattering albedo, MRF Tech. Note 31, 2000. (Available from Met. Off., Bracknell, UK).

Haywood, J. M., and V. Ramaswamy, Global sensitivity studies of the direct radiative forcing of sulfate and black carbon aerosol, *J. Geophys. Res.*, *103*, 6043–6058, 1998.

Haywood, J. M., D. L. Roberts, A. Slingo, J. M. Edwards, and K. P. Shine, General circulation model calculations of the direct radiative forcing by anthropogenic sulphate and fossil-fuel soot aerosol, *J. Clim.*, *10*, 1562–1577, 1997.

Haywood, J. M., P. N. Francis, M. D. Glew, and J. P. Taylor, The optical properties and direct radiative effect of Saharan Dust: A case study of two Saharan dust outbreaks using aircraft data, *J. Geophys. Res.*, *106*, 18,417–18,428, 2001a.

Haywood, J. M., P. N. Francis, I. Geogdzhayev, M. Mishchenko, and R. Frey, Comparison of Saharan Dust aerosol optical depth derived using aircraft mounted pyranometers and 2-channel AVHRR retrieval algorithms, *Geophys. Res. Lett.*, *28*(12), 2393–2396, 2001b.

Haywood, J. M., P. N. Francis, M. D. Glew, O. Dubovik, and B. N. Holben, Comparison of aerosol size distributions, radiative properties and optical depths determined by aircraft observations and sunphotometers during SAFARI 2000, *J. Geophys. Res.*, *108*, doi:10.1029/2002JD002250, in press, 2003a.

Haywood, J. M., P. Francis, S. Osborne, M. Glew, N. Leob, E. Highwood, D. Tanré, G. Myhre, and P. Formenti, Radiative properties and direct radiative effect of Saharan dust measured by the C-130 aircraft during SHADE, 1, Solar spectrum, *J. Geophys. Res.*, *108*, doi:10.1029/2002JD002687, in press, 2003b.

Herman, J. R., P. K. Bhartia, O. Torres, C. Hsu, C. Seftor, and E. Celarier, Global distribution of UV-absorbing aerosols from Nimbus-7 TOMS data, *J. Geophys. Res.*, *102*, 16,911–16,922, 1997.

Hignett, P., J. P. Taylor, and P. N. Francis, Comparison of observed and modeled direct aerosol forcing during TARFOX, *J. Geophys. Res.*, *104*, 2279–2287, 1999.

Hirst, E., P. H. Kaye, R. S. Greenaway, P. Field, and D. W. Johnson, Discrimination of micrometre-sized ice and super-cooled droplets in mixed-phase cloud, *Atmos. Environ.*, *35*, 33–47, 2001.

Hobbs, P. V., J. S. Reid, R. A. Kotchenruther, R. J. Ferek, and R. Weiss, Direct radiative forcing by smoke from biomass burning, *Science*, *275*, 1776–1778, 1997.

Holben, B. N., et al., AERONET: A federated instrument network and data archive for aerosol characterization, *Remote Sens. Environ.*, *66*, 1–16, 1998.

Horvath, H., Atmospheric light absorption: A review, *Atmos. Environ.*, *27A*, 293–317, 1993.

IPCC (Intergovernmental Panel on Climate Change), *Climate Change 2001: The Scientific Basis*, edited by J. T. Houghton et al., pp. 36–46, Cambridge Univ. Press, New York, 2001.

Johnson, D. W., et al., An overview of the Lagrangian experiments undertaken during the North Atlantic Aerosol Characterisation Experiment (ACE-2), *Tellus*, *52B*, 290–320, 2001.

Keil, A., and J. M. Haywood, Solar radiative forcing by biomass aerosol particles over marine clouds during SAFARI 2000: A case study based on measured aerosol and cloud properties, *J. Geophys. Res.*, *108*, doi:10.1029/2002JD002315, in press, 2003.

Knollenberg, R. G., The measurement of latex particle sizes using scattering ratios in the Rayleigh scattering range, *J. Aerosol Sci.*, *3*, 331–345, 1989.

Kotchenruther, R. A., and P. V. Hobbs, Humidification factors of aerosols from biomass burning in Brazil, *J. Geophys. Res.*, *103*, 32,081–32,089, 1998.

Le Canut, P., M. O. Andreae, G. W. Harris, F. G. Wienhold, and T. Zenker, Airborne studies of emissions from savanna fires in southern Africa, 1, Aerosol emissions measured with a laser optical particle counter, *J. Geophys. Res.*, *101*, 23,615–23,630, 1996.

Liu, P. S. K., W. R. Leaitch, J. W. Strapp, and M. A. Wasey, Response of particle measuring systems airborne ASASP and PCASP to NaCl and latex particles, *Aerosol Sci. Technol.*, *16*, 83–95, 1992.

Magi, B., and P. V. Hobbs, Effects of humidity on aerosols and southern Africa during the biomass burning season, *J. Geopys. Res.*, *108*, doi:10.1029/2002JD002144, in press, 2003.

Martins, J. V., P. Artaxo, C. Liousse, J. S. Reid, P. V. Hobbs, and Y. Kaufman, Effects of black carbon content, particle size, and mixing on light absorption by aerosols from biomass burning in Brazil, *J. Geophys. Res.*, *103*, 32,041–32,050, 1998.

Mayol-Bracero, O. L., P. Guyon, B. Graham, G. Roberts, M. O. Andreae, S. Decesari, M. C. Facchini, S. Fuzzi, and P. Artaxo, Water-soluble organic compounds present in biomass burning aerosols over Amazonia, 2, Apportionment of the chemical composition and importance of the polyacidic fraction, *J. Geophys. Res.*, *107*(D20), 8091, doi:10.1029/2001JD000522, 2002.

Myhre, G., F. Stordal, K. Restad, and I. Isaksen, Estimates of the direct radiative forcing due to sulfate and soot aerosols, *Tellus, Ser. B*, *50*, 463–477, 1998.

Myhre, G., T. Berntsen, F. Stordal, and J. M. Haywood, Modeling the solar radiative impact of aerosols from biomass burning during SAFARI-2000, *J. Geophys. Res.*, *108*, doi:10.1029/2002JD002313, in press, 2003.

Penner, J. E., et al., Aerosols, their direct and indirect effects, in *Climate Change 2001: The Scientific Basis: Contribution of Working Group I to the Third Assessment Report of the Intergovernmental Panel on Climate Change*, edited by J. T. Houghton et al., pp. 291–348, Cambridge Univ. Press, New York, 2001.

Ramaswamy, V., O. Boucher, J. Haigh, D. Hauglustaine, J. M. Haywood, G. Myhre, T. Nakajima, G. Y. Shi, and S. Solomon, Radiative Forcing of Climate Change, in *Climate Change 2001: The Scientific Basis: Contribution of Working Group I to the Third Assessment Report of the Intergovernmental Panel on Climate Change*, edited by J. T. Houghton et al., pp. 349–416, Cambridge Univ. Press, New York, 2001.

Reid, J. S., and P. V. Hobbs, Physical and optical properties of young smoke from individual biomass fires in Brazil, *J. Geophys. Res.*, *103*, 32,013–32,030, 1998.

Reid, J. S., P. V. Hobbs, C. Liousse, J. V. Martins, R. E. Weiss, and T. F. Eck, Comparisons of techniques for measuring shortwave absorption and black carbon content of aerosols from biomass burning in Brazil, *J. Geophys. Res.*, *103*, 32,031–32,040, 1998a.

Reid, J. S., P. V. Hobbs, R. J. Ferek, D. R. Blake, J. V. Martins, M. R. Dunlap, and C. Liousse, Physical, chemical and optical properties of regional hazes dominated by smoke in Brazil, *J. Geophys. Res.*, *103*, 32,059–32,080, 1998b.

Remer, L. A., Y. J. Kaufman, B. N. Holben, and A. M. Thompson, Biomass burning aerosol size distribution and modeled optical properties, *J. Geophys. Res.*, *103*, 31,879–31.891, 1998.

Ross, J. L., P. V. Hobbs, and B. Holben, Radiative characteristics of regional hazes dominated by smoke from biomass burning in Brazil: Closure tests and direct radiative forcing, *J. Geophys. Res.*, *103*, 31,925–31,941, 1998.

Ruellan, S., H. Cachier, A. Gaudichet, P. Masclet, and J. P. Lacaux, Airborne aerosols over central Africa during the Experiment for Regional Sources and Sinks of Oxidants (EXPRESSO), *J. Geophys. Res.*, *104*, 30,673–30,690, 1999.

Schmid, H., et al., Results of the "carbon conference" international aerosol carbon round robin test stage I, *Atmos. Environ.*, *35*, 2111–2121, 2001.

Sokolik, I. N., and O. B. Toon, Direct radiative forcing by anthropogenic airborne mineral aerosols, *Nature*, *381*, 681–683, 1996.

Strapp, J. W., W. R. Leaitch, and P. S. K. Liu, Hydrated and dried aerosol-size distribution measurements from the particle measuring systems FSSP-300 probe and the deiced PCASP-100X probe, *J. Atmos. Oceanic Technol.*, *9*, 548-555, 1992.

World Climate Program (WCP), *A Preliminary Cloudless Standard Atmosphere for Radiation Computation*, World Meteorol. Organ., Geneva, 1986.

Yamasoe, M. A., Y. J. Kaufman, O. Dubovik, L. A. Remer, B. N. Holben, and P. Artaxo, Retrieval of the real part of the refractive index of smoke particles from Sun/sky measurements during SCAR-B, *J. Geophys. Res.*, *103*, 31,893–31,902, 1998.

M. O. Andreae, Max Planck Institute for Chemistry, P.O. Box 3060, D-55020 Mainz, Germany.

P. Formenti, Centre of Geophysics, University of Evora, Rua R. Ramalho, 59, P-7000-532 Evora, Portugal.

P. N. Francis, J. M. Haywood, A. Keil, and S. R. Osborne, Meteorological Office, Y46 Building, Cody Technology Park, Farnborough, GU14 0LX, UK. (jim.haywood@metoffice.com)

P. H. Kaye, STRC, University of Hertfordshire, Hatfield, AL10 9AB, UK.